ADVANCED FUNCTIONAL MATERIALS
www.afm-journal.de

Hydrophobic Deep Eutectic Solvent (DES) Design Enables Optimally Hydrated DES-in-Water Electrolytes for High-Performance Bromine Redox-Enhanced Energy Storage Systems

*Tae Pyeong Eom, Gunwoo Lee, Young Hun Cho, Younjee Lim, and Seung Joon Yoo**

Supercapacitors are renowned for rapid charging, high power density, and long lifespan, yet their practical applications are limited by low energy densities. Redox-enhanced electrochemical capacitors (redox ECs) address this limitation by incorporating redox-active electrolytes, enabling Faradaic charge storage. Bromide is a promising catholyte due to its high reduction potential, excellent solubility, and low cost. However, the generation of corrosive Br_2 and the cross-diffusion of soluble polybromides result in suboptimal cell efficiency including severe self-discharge and reduced cycle life. Although solid complexing agents have been used to suppress polybromides' cross-diffusion, this approach necessitates water, which inherently limits electrochemical and thermal stability. Here, a hydrated deep eutectic solvent (HDES) electrolyte is developed by combining tetrabutylammonium bromide (TBAB) with ethylene glycol. This HDES system effectively utilizes the multifunctional roles of TBAB: the bromide anion functions as a catholyte, while the TBA cation suppresses polybromides' cross-diffusion as a built-in solid complexing agent. Critically, unlike previous studies that focus on minimally hydrated DESs, this system leverages the hydrophobic effect of TBAB to accommodate higher water content, addressing challenges inherent to DESs while maintaining superior electrochemical and thermal stability. The optimized HDES-50 electrolyte, containing 50 wt.% water, provides a robust and efficient solution for advanced redox ECs.

1. Introduction

The depletion of fossil fuels and growing environmental concerns drive the demand for sustainable energy sources. However, the intermittent availability of renewable energy sources poses a challenge in maintaining a reliable energy supply, highlighting the importance of energy storage. Among various electrochemical energy storage systems, supercapacitors are widely used across multiple fields due to their rapid charging rate, high power density, and long cycle life.[1] These advantageous properties make them ideal for integration into mobile devices, hybrid electric vehicles, and wearable devices.[2] However, their comparatively lower energy density compared to secondary batteries has prompted the development of energy-density-augmented supercapacitors.[3]

Redox-enhanced electrochemical capacitors (redox ECs) utilize reversible oxidation-reduction reactions of dissolved redox-active species for Faradaic charge storage while employing electric double layers for capacitive charge storage. This hybrid approach aims to combine the benefits of high power density and long cycle life with improved energy density, addressing the limitations of supercapacitors. Among the various redox couples, aqueous bromine electrolytes stand out for their cost-effectiveness, high solubility, and high reduction potential ($Br_2 + 2e^- \leftrightarrow 2Br^-$; 1.08 V vs SHE) with electrochemical reversibility, making them promising catholytes in redox-employed systems.[4] However, the charging process in bromide-based systems generates corrosive and volatile bromine/polybromide species ($Br_2 + Br^- \rightarrow Br_3^-$). The cross-diffusion of these species results in suboptimal coulombic efficiency and severe self-discharge, posing significant challenges to commercialization.[4c,5] To overcome these issues, previous studies have introduced additives that form complexes with the polybromide species in the aqueous electrolyte to mitigate the unwanted reactivity and polybromides' cross-diffusion.[6]

Tetrabutylammonium bromide (TBAB) is widely recognized in redox ECs as an effective bromine complexing agent.[4b,7] During the charging process, TBA^+, characterized by its long alkyl chains, interacts with tribromide (Br_3^-) ions to form a solid [$TBA^+ \bullet Br_3^-$] complex. This solid complex formation, driven by dehydration of the hydrophobic [$TBA^+ \bullet Br_3^-$] hydrated droplet, effectively prevents the cross-diffusion of Br_3^- and suppresses

T. P. Eom, G. Lee, Y. H. Cho, Y. Lim, S. J. Yoo
School of Materials Science and Engineering
Gwangju Institute of Science and Technology
Gwangju 61005, Republic of Korea
E-mail: sjoonyoo@gist.ac.kr

The ORCID identification number(s) for the author(s) of this article can be found under https://doi.org/10.1002/adfm.202424243

DOI: 10.1002/adfm.202424243

self-discharge.[7b] As the hydration and dehydration processes are pivotal for complex formation, a sufficient amount of water in the electrolyte environment is necessary. Consequently, TBAB and similar additives are used exclusively in aqueous electrolytes to ensure effective solid complex formation.

Nevertheless, aqueous bromine-based systems encounter challenges related to both electrochemical and thermal instability, which are inherent to aqueous electrolytes. Aqueous systems are constrained by a narrow electrochemical stability window (ESW) due to water decomposition reactions occurring within a limited voltage window (1.23 V).[8] These reactions can result in gas evolution and electrode degradation. Additionally, the volatility and thermal instability of aqueous electrolytes compromise reliability, especially when operating at elevated temperatures.[9] Therefore, there is a pressing need to develop electrolyte systems that offer improved stability while retaining the advantages of aqueous systems.

Deep eutectic solvents (DESs) have emerged as a promising alternative electrolytes. DESs, formed through intermolecular hydrogen bonding between hydrogen bond donors and acceptors, provide a wide ESW, as well as chemical and thermal stability.[10] However, their practical application in energy storage is hindered by high viscosity and low ionic conductivity. To improve these electrolyte properties, hydrated DESs (HDESs) have been explored, where the addition of water reduces viscosity and enhances ionic conductivity.[11] Yet, prior HDES formulations incorporated only a small fraction of water, rendering them ineffective in fully retaining the advantages of aqueous systems.[10b,12]

In this work, we present an electrolyte engineering strategy that bridges the benefits of aqueous and non-aqueous electrolytes. We first developed a DES by mixing ethylene glycol (EG) with TBAB as eutectic electrolyte components. Unlike previous studies where TBAB served only as an additive, here it functions as a DES component, bromide source, and built-in complexing agent, simplifying electrolyte composition and preparation. Recognizing that sufficient water is essential for TBAB to effectively form a solid complex with Br_3^-, as well as to lower viscosity and increase conductivity, we deliberately advanced this system into a water-rich eutectic mixture. Prior studies have investigated the structural evolution of DES-water mixtures, demonstrating that beyond a certain dilution threshold, the DES network is disrupted, leading to a transition where water dominates the solution properties.[13] While these studies have provided valuable insights into DES solvation dynamics and phase segregation, the application of DES-water mixtures in energy storage remains an area for further exploration. Our TBAB-based HDES system strategically utilizes this transition by leveraging the hydrophobic effect of TBAB. The formation of a hydrophobic layer at the anode prevents direct water contact, enabling higher water content accommodation. This approach achieves an optimal balance of bromine complexation, viscosity, and ionic conductivity, mitigating challenges inherent to DES while also addressing issues in aqueous systems. The optimized hydration level also improves mass transfer characteristics and electrochemical kinetics without compromising ESW.

We fabricated redox ECs using activated porous carbon electrodes to investigate the performance of the optimized HDES electrolyte (50 wt.% water content). The high coulombic efficiency observed is attributed to suppressed self-discharge, facilitated by effective bromine complexation and increased ionic conductivity. Superior cycle life was demonstrated through both floating and high-temperature tests, highlighting the electrolyte's stability. To further assess the compatibility and long-term cycle stability of the HDES in a high-performance dual redox EC, a full-cell was assembled, using butyl viologen (BV) as the anolyte to match the capacity of the bromide catholyte. This system achieved a coulombic efficiency of 97.5%, energy density of 36.3 Wh kg^{-1} and retained 87% of its energy density after 10 000 cycles (1730 h).

2. Results and Discussion

Figure 1a,b illustrate the issues at the anode and cathode for bromine-based aqueous and DES electrolytes, respectively. For the efficient operation of an aqueous bromine redox system, the following issues need to be addressed. 1) water decomposition reaction leading to reduced coulombic efficiency and electrolyte consumption at the anode (Figure 1a); 2) the cross-diffusion of Br_3^- causing self-discharge and corrosion at the cathode (Figure 1b). These issues result in shortened lifespans and decreased efficiency. While DESs can prevent water-triggered side reactions of aqueous electrolytes, they still struggle to address charged bromide cross-diffusion due to insufficient bromine complexation in non-aqueous solutions (Figure 1b). By formulating a TBAB-based HDES, the aforementioned issues at both the anode and cathode can be addressed simultaneously, as shown in Figure 1c. At the cathode, the tetrabutylammonium cation of TBAB serves as a bromine complexing agent (see details in the Note S1, Supporting Information), while at the anode, it forms a hydrophobic layer that inhibits water decomposition reactions.[7b] Furthermore, TBAB functions as a bromide catholyte, enabling Faradaic charge storage without the need for additional redox species, thus simplifying the electrolyte composition.

The DES was prepared by mixing TBAB and EG at a molar ratio of 1:3. The mixture was heated at 80 °C with continuous stirring until a homogeneous, colorless liquid formed (Figure 1d; S1a, Supporting Information).[14] To prepare HDES electrolytes, varying amounts of water (e.g., 10%, 30%, and 50% by weight–designated as HDES-10, HDES-30, and HDES-50, respectively) were added, resulting in DES-water mixtures with various hydration levels (Figure S1b, Supporting Information). To maintain clarity and precision in our classification, we define HDESas a broad term encompassing all water-DES mixtures, regardless of their water content. This terminology provides a comprehensive framework that accounts for varying hydration levels while ensuring consistency in nomenclature.

Intermolecular hydrogen bonding can induce perturbations in bond length and strength. To investigate structural changes driven by hydrogen bonding interactions in DES, Raman spectroscopy and Fourier-transform infrared spectroscopy (FTIR) were employed. Raman spectra of neat EG showed broad bands centered at ≈3350 cm^{-1}, corresponding to the O—H stretching vibrations (Figure 1e-orange).[15] When mixed with TBAB during DES formation, the O—H stretching vibration peak of EG showed a blueshift (Figure 1e-green), indicating that intermolecular hydrogen bonds of EG itself were gradually disrupted while restructured hydrogen bonding network formed between the bromine

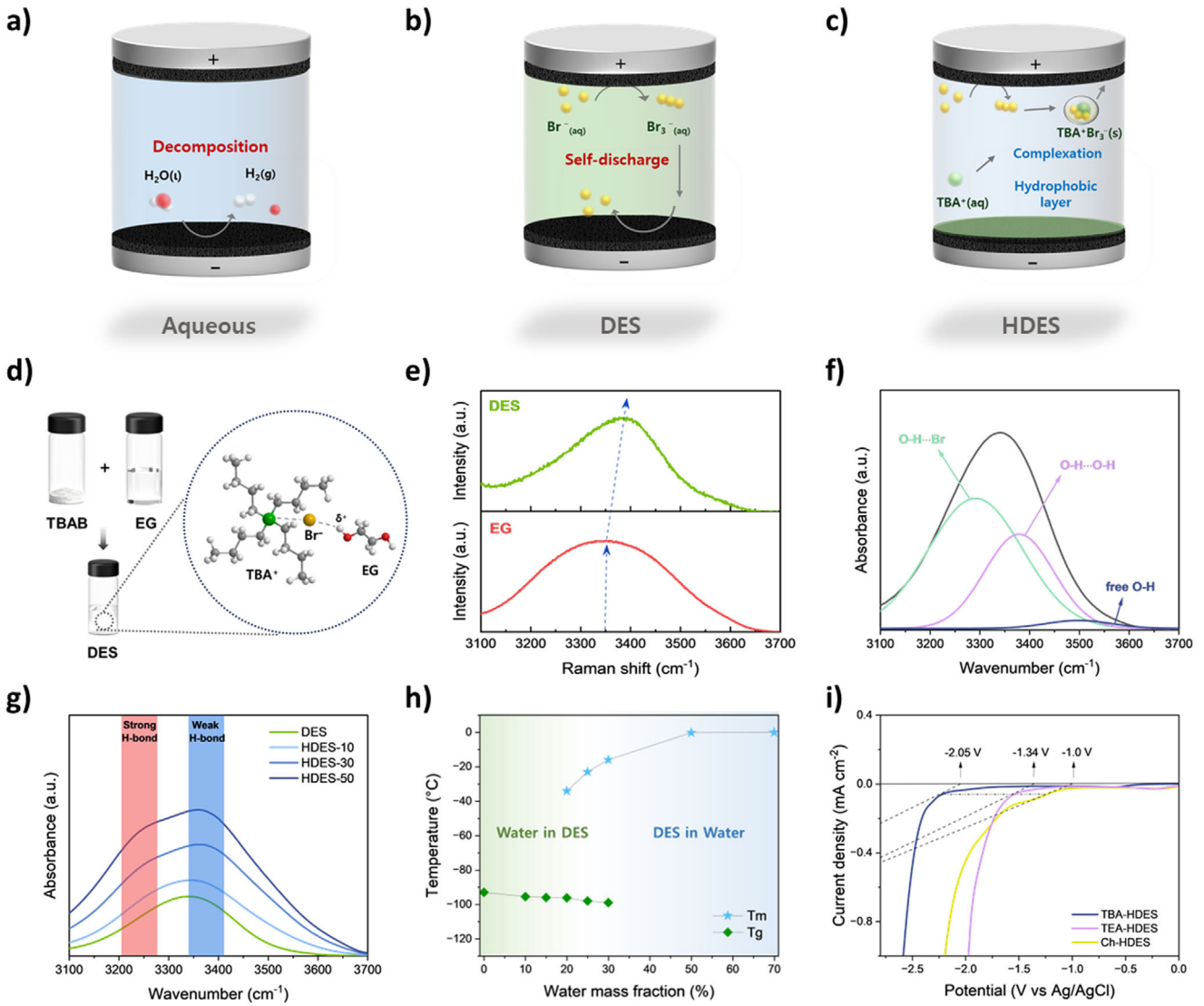

Figure 1. Properties of HDES electrolytes compared to DES. a–c) Schematic illustrations of challenges in a) aqueous, b) DES, and c) HDES electrolytes in bromine-based redox systems, with HDES addressing the limitations of the other systems. d) Preparation of DES, with a zoomed-in view illustrating intermolecular interactions between components. e) Raman spectra confirming DES formation through the O—H stretching peak. f) Deconvoluted FTIR spectra of the ν (O—H) peak in DES. g) Comparative FTIR spectra of various electrolytes, highlighting the ν (O—H) region for DES and HDES-10, HDES-30, and HDES-50 formulations. h) Transition from water-in-DES to DES-in-water as a function of water mass fraction. i) Linear sweep voltammetry (LSV) curves of various HDES electrolytes with differently structured quaternary ammonium cations.

ions of TBAB and the hydroxyl group of EG. In the FTIR analysis, the spectrum of DES was further examined in the range of 3100–3700 cm^{-1}, focusing on the O—H stretching region. Deconvolution of the spectrum resolved overlapping peaks, allowing for the identification of distinct contributions from various types of O-H stretching vibrations (Figure 1f). The peak at 3249 cm^{-1} corresponds to O—H···Br interactions, indicative of hydrogen bonding interactions between the O-H groups of EG and bromide ions (Figure 1f-green; Figure S2, Supporting Information). The peaks at 3363, and 3499 cm^{-1} were attributed to the intermolecular O—H···O—H interactions (purple curve) and the stretching vibration of free OH groups (blue curve), respectively.[16] The former suggests hydrogen bonding between neighboring O—H groups within the DES structure, while the latter corresponds to non-bonded O—H groups in EG. This result aligns with the classification of type III DES formation where an organic salt interacts with a hydrogen bonding donor, leading to a distinct rearrangement of the hydrogen bonding network that stabilizes the DES structure.[17]

We investigated the structural changes from DES to HDES with varying amounts of water added. The FTIR spectrum shows that as the amount of water added to DES increases (from HDES-10 to HDES-50), the ratio of strong hydrogen bonds to weak hydrogen bonds in the O—H peak increases as the incorporation of water introduces dense hydrogen bond interactions between water and DES components (Figure 1g).[11a,18] Additional Raman comparisons between HDESs and DES showed no significant changes in peak positions, except for slight blueshifts

in the O—H peaks at 3100–3700 cm^{-1}, indicating alterations in hydrogen bonding (Figure S3, Supporting Information). These combined spectroscopic results provide evidence that water functions as both a hydrogen bond donor and acceptor, playing a crucial role as a component in the DES structure through hydrogen bonding.[19]

In the HDES, the structural network of the electrolyte shifts with the hydration level. Numerous studies have extensively examined hydration-driven structural and physicochemical transformations in DESs. A diverse range of analytical techniques including differential scanning calorimetry (DSC), nuclear magnetic resonance (NMR) spectroscopy, Brillouin spectroscopy, and molecular dynamics simulations, has been employed to provide a comprehensive understanding of how increasing water content disrupts the hydrogen bonding network and modifies the solvation environment in DESs.[13c,20] At low hydration levels, the DES primarily acts as a network host, dictating the system's structure and properties, representing a "water-in-DES" regime. Conversely, at high hydration levels, water plays a dominant role in governing the overall structure and behavior of the system, transitioning it into a "DES-in-water" state, where the system predominantly exhibits aqueous-like properties rather than those of a DES.[20c] To investigate the thermal properties of DES electrolytes across varying water contents (10, 15, 20, 25, 30, 50, and 70 wt.%), DSC measurements were conducted. For water contents of 15 wt.% and below, no thermal events were observed except for the glass transition, indicating that the DES behaves as an amorphous liquid (Figures S4 and S5, Supporting Information). At these low hydration levels, water participates in hydrogen bonding within the DES structure. At high hydration levels, however, water can solvate each component of the DES, progressively disrupting its structured network and ultimately imparting the intrinsic properties of an aqueous system.[19,21] When water content reaches 20 wt.% or more, melting transitions were observed between −34 and 0 °C, and crystallization peaks were observed between −54 and −27 °C (Figure S4, Supporting Information). These transitions are likely due to the behavior of free water that is not integrated into the hydrogen-bond network of the DES structure. HDES electrolytes that did not exhibit melting and crystallization peaks are classified as water-in-DES, whereas those displaying these peaks are categorized as DES-in-water (Figure 1h). This variation in thermal behavior highlights a critical trade-off: while higher hydration levels enhance the ionic conductivity of DES systems, water-rich HDES are not suitable as electrolytes due to water-triggered side reactions, which significantly compromise both electrochemical and cycle stability.[10b,12] Consequently, HDES systems have typically been employed within a limited range of water content, restricting their capacity to fully exploit the advantages of aqueous electrolytes.

The integration of water-rich HDES (DES-in-water) as an electrolyte to achieve a wide ESW is an important yet challenging consideration. Suppressing the hydrogen evolution reaction (HER) is critical in this context. We hypothesize that the hydrophobic nature of TBAB enhances electrochemical stability, facilitating the integration of DES-in-water as an electrolyte by forming a protective layer at the anode. This layer prevents direct water contact, thereby suppressing the HER and water-triggered side reactions, while still retaining the benefits of water, such as high ionic conductivity, and maintaining electrolyte stability. To validate this hypothesis and demonstrate the hydrophobic effect of TBAB at the anode, LSV measurements were conducted to compare the HER suppression capabilities of electrolytes containing different hydrophobic cations. Tetraethylammonium (TEA^+) and choline (Ch^+), which are less hydrophobic than TBA^+ and commonly used as DES components, were included for comparison (structures shown in Figure S6, Supporting Information). These cation-based HDESs were prepared by mixing each cation and EG at a molar ratio of 1:3, followed by the addition of water to achieve a 1:1 mass ratio of DES to water (Figure S7, Supporting Information). To determine the onset potential of the HER for each electrolyte, tangent lines were drawn at 0.06 mA cm^{-2} on the LSV curves.[22] The onset HER potentials were identified at the intersection of these tangent lines with the y = 0 axis. As shown in Figure 1i, a higher hydrophobicity associated with longer alkyl chain lengths ($TBA^+ > TEA^+ > Ch^+$) corresponded to a wider ESW. When a voltage is applied, these hydrophobic cations accumulate at the negatively charged anode surface, forming a protective layer that prevents water from accessing the interfacial region, thereby inhibiting water-triggered side reactions.[22,23] Consequently, TBAB functions as an effective protective agent, allowing the use of DES-in-water electrolytes without compromising electrochemical stability.

To design an optimal electrolyte for systems utilizing bromide as a catholyte, a thorough evaluation of the advantages and disadvantages of incorporating water is essential for determining the optimal hydration level. We systematically investigated the physicochemical and electrochemical properties of TBA-EG-based DES as a function of water content.

A fast self-discharge due to bromine cross-diffusion is a critical issue, which can be mitigated by adding a bromine complexing agent. TBAB is well known for its ability to form solid bromine complexes.[7,24] Notably, water plays a crucial role in this solid complexation process. The chemical formation of the [TBA^+•Br_3^-] solid complex was monitored by adding a uniform amount of Br_3^- aqueous solution to DES, HDESs, and an aqueous 1 M TBAB solution (Figure S8, Supporting Information).[4b,25] Among the HDES electrolytes, bromine complexes were formed in HDES-50, whereas no solid complex formation occurred in HDES-10 and HDES-30, which contain low water content (**Figure 2a**). These results indicate that HDES within the DES-in-water range facilitates solid-state bromine complexation. To further confirm the formation of the solid complex in HDES-50 and verify its electrochemical generation, we conducted a constant-current electrolysis.[4b] This experiment confirmed the electrochemical formation of the [TBA^+•Br_3^-] solid complex on the electrode in the HDES-50 electrolyte (Figure S9, Supporting Information), suggesting that utilizing HDES within the DES-in-water range can effectively inhibit the cross-diffusion of Br_3^-.

In addition, incorporating sufficient water content into the electrolyte retains key advantages of aqueous solutions such as non-flammability, low viscosity, and high ionic conductivity. A flammability test was conducted by soaking each solution in the separator and then igniting it (Figure 2b). While the organic EG and EG-based DES electrolytes ignited readily, the HDES-50 electrolyte did not catch fire. This result demonstrates that the inclusion of water in the DES system contributes to its

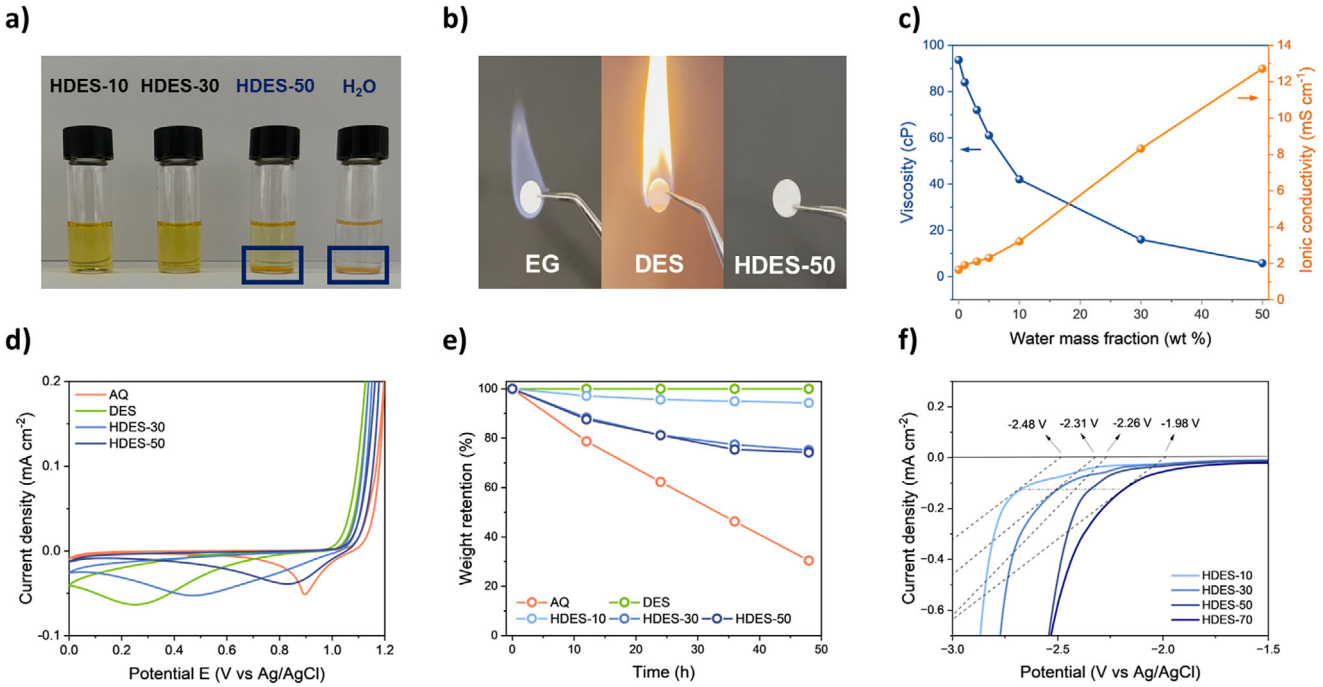

Figure 2. Water-content-dependent physicochemical and electrochemical properties. a) Br_3^- complexation test of HDES electrolytes versus water (1 M TBAB) after the addition of chemically generated Br_3^-. b) Snapshots of glass fiber after exposing it to an open frame for 5 s with different electrolytes. c) Viscosity and conductivity of electrolytes with varying water contents. d) Cyclic voltammograms of electrolytes with different water contents. e) Weight retention of various electrolytes with different water contents. f) LSV curves of HDESs with varying water contents.

non-flammability. With 50% water content, the HDES-50 electrolyte achieves non-flammability, making it suitable for a broad range of applications. We also compared the viscosity and ionic conductivity of DES and HDES electrolytes (Figure 2c). The pure DES exhibited a high viscosity of 93.67 cP and a low ionic conductivity of 1.64 mS cm^{-1}. As the water content increased, viscosity markedly decreased while ionic conductivity improved. Notably, the HDES-50 electrolyte exhibited a low viscosity of 5.78 cP and a high ionic conductivity of 12.71 mS cm^{-1}, underscoring its enhanced suitability for practical applications requiring high power performance. Next, cyclic voltammetry (CV) analysis was performed to evaluate the bromide redox reaction. The HDES-50 electrolyte demonstrated a more reversible bromide redox reaction (Figure 2d) whereas electrolytes with low water content showed a significant cathodic shift of reduction peaks, greater peak-to-peak separation, and sluggish redox kinetics. These effects are attributed to the low ionic conductivity caused by strong hydrogen bonding between DES components.[26]

One of the key advantages of optimal HDES is its robust thermal stability, derived from the inherent properties of DES, which addresses the issue of rapid evaporation in aqueous electrolytes. The low vapor pressure of pure DES prevents discharge capacity decay over time. To assess how this property varies with water content, electrolytes were exposed to the open atmosphere at 25 °C (Figure 2e).[11c,27] The DES electrolyte exhibited exceptionally low volatility, showing no significant weight loss after 48 h. In contrast, the aqueous electrolyte showed a high evaporation rate, with a weight retention of only 30.36%. Notably, HDES-50 retained 74.2% of its weight, indicating enhanced thermal stability compared to conventional aqueous electrolytes.

While HDES can mitigate several limitations of DES, excessive water content can introduce drawbacks. As shown in Figure 2f, increasing the water content in TBAB/EG-based DES reduces ESW, primarily due to the dilution of TBAB concentration, which weakens the hydrophobic effect (Figure S10, Supporting Information). For instance, in HDES-70, the TBAB concentration falls below 1 M, increasing susceptibility to the HER, with an onset HER potential of −1.72 V (vs Ag/AgCl). Nevertheless, HDES-50 maintains a cathodic stability window extending beyond −2 V (vs Ag/AgCl), achieving the optimal balance between hydration level and electrochemical stability.

A thorough analysis of water's role in HDES and the optimization of multiple electrolyte parameters are crucial for developing a well-balanced electrolyte that enhances overall cell performance. With its optimal balance of hydration level and key physicochemical and electrochemical stability, HDES-50 is identified as the most suitable electrolyte for improving the efficiency and stability of practical redox RC systems.

To validate the favorable electrolyte properties of HDES-50 in practical battery applications, full-cell evaluations were conducted using an asymmetric cell setup. An asymmetric setup allows one electrode (typically a capacitive electrode) to be oversized to ensure that the redox-active electrode reaches its full potential range. In this work, by increasing the anode mass (a 3:1 anode-to-cathode mass ratio), the capacitive charge stored at the anode is increased, ensuring that it can accommodate the charge contribution from the cathode. This configuration allows for an uninterrupted examination of the bromine-based Faradaic charging process (Figure S11, Supporting Information), preventing voltage

limitations that would otherwise be imposed by a smaller counter electrode.

CV measurements were performed to evaluate the electrochemical behavior of HDES-50 and DES electrolytes. The CV curves of HDES-50 electrolytes displayed higher current densities, indicating larger charge storage capacity compared to DES at all scan rates (**Figure 3a**; Figure S12, Supporting Information). These enhancements are closely linked to the ion diffusion and charge transfer characteristics of the electrolyte, as revealed by electrochemical impedance spectroscopy (EIS) measurements (Figure 3b). In the high-frequency region, the HDES electrolytes exhibit lower values of R_s (solution resistance) and R_{ct} (charge transfer resistance) compared to DES, indicating reduced resistance to ion movement and faster charge transfer kinetics. Warburg diffusion behavior was observed in the low-frequency region. Calculating the Warburg coefficient (σ) from the EIS data shows that the HDES electrolyte has a lower value of 21.79, compared to 80.37 for DES (Figure S13, Supporting Information).[28] This lower Warburg coefficient reflects faster ion diffusion and reduced ion diffusion resistance.

To investigate charge storage behavior, galvanostatic charge–discharge (GCD) cycling tests were conducted using a three-electrode configuration. In both DES and HDES electrolytes, the respective GCD curves exhibited a Faradaic plateau at the cathode, corresponding to the bromide redox reaction (Figure 3c,d). At the anode, a linear potential profile was observed, indicative of capacitive charging. A notable difference in ohmic potential drop (IR drop) was observed between DES and HDES, which is further examined in the rate capability test section.

Self-discharge rates of each electrolyte were assessed through open-circuit self-discharge tests, where voltage retention and capacity retention were monitored over time after fully charging the cells. While the DES electrolyte experienced significant capacity loss during the initial stage of the self-discharge test, HDES-50 electrolyte exhibited superior performance, maintaining 50.5% voltage retention and 52.9% capacity retention after 8 h, outperforming both DES (17% voltage retention, 28.5% capacity retention) and HDES-30 (27% voltage retention, 41% capacity retention) (Figure 3e,f). Interestingly, HDES-30, which falls within the water-in-DES range proved ineffective at preventing the cross-diffusion of polybromide species.

To further elucidate the effectiveness of Br_3^- cross-diffusion inhibition in HDES-50, we conducted H-type cell experiments using a transparent setup (Figure 3g), allowing for real-time visualization of polybromides diffusion. In the HDES-50 electrolyte system, the yellow-colored Br_3^- species did not diffuse freely within the electrolyte but instead interacted with TBA^+, forming a solid complex that deposits onto the activated carbon electrode, effectively mitigating cross-diffusion of Br_3^- (Figure S14, Supporting Information).

To assess Br_3^- retention over an extended period, the solution from the anode chamber was analyzed seven days post-charging using a potassium iodide (KI) paper test and UV–vis spectroscopy (Figure 3h,i). KI paper is highly sensitive to Br_2, undergoing a color change at concentrations as low as 0.005 mM, serving as a reliable indicator of bromine diffusion.[7d,29] In the HDES-50 electrolyte, even after 7 days, the KI paper remained unaltered, demonstrating that Br_3^- cross-diffusion to the opposing electrode was effectively suppressed (Figure 3i).

For quantitative validation, an electrolyte sample was extracted from the anode chamber and analyzed using UV–vis spectroscopy. Notably, in HDES-50, no polybromide-related absorption peaks were detected, further corroborating the suppression of Br_3^- cross-diffusion (Figure 3h). The results from both KI paper analysis and UV–vis measurements consistently confirm the efficient inhibition of Br_3^- cross-diffusion in HDES-50. These findings establish a direct correlation between the bromine complexing ability observed in Figure 2a and the electrolyte's capacity to suppress self-discharge (Figure 3f).

To further evaluate the electrochemical performance of HDES-50, rate capability tests were conducted using a two-electrode cell configuration, with GCD measurements performed over a current density range of 0.25 to 10 A g^{-1} (Figure 3j,k). DES exhibited an IR drop of 235, 432, 660, 765, 998, and 1000 mV at testing current densities from 0.25 to 10 A g^{-1}, respectively (Figure S15, Supporting Information). In contrast, HDES-50 showed a significantly lower IR drop across all current rates (Figure S16, Supporting Information). To further quantify this effect, equivalent series resistance (ESR) was calculated from the IR drop at the initial stage of the discharging curve from the GCD test, revealing that HDES-50 has an ESR of 83.3 Ω, whereas DES exhibits a substantially higher ESR of 141.7 Ω when cycled at 10 A g^{-1} (Figure S17, Supporting Information). This reduction in IR drop and ESR in HDES-50, resulting from its lower resistance and enhanced ionic conductivity, leads to better electrochemical performance, enabling a higher energy density of 39.5 Wh kg^{-1} at 1 A g^{-1} (Figure 3j).[30] While HDES-50 shows a more noticeable energy decrease at higher current densities, this behavior does not negate its superior rate capability as it retains higher energy and efficiency across all cycling conditions (Figure S18, Supporting Information).

Additionally, the HDES-50 electrolyte maintained high coulombic efficiency of 98.7%, 99.5%, 99.3%, and 99.1% at 1, 2, 5, and 10 A g^{-1}, respectively, due to its ability to suppress cross-diffusion (Figure 3k). In contrast, the DES electrolyte exhibited notably lower coulombic efficiency across all rates, with 87.5% at 1 A g^{-1}. This poor performance is largely attributed to the insufficient bromine complexation ability, consequently resulting in severe cross-diffusion of Br_3^-, which is strongly linked to the decreased energy efficiency observed in DES (Figure S18, Supporting Information). The water-rich HDES-50 electrolyte demonstrates remarkable enhancements in charge storage capacity, ion diffusion, and self-discharge suppression, driven by its superior ionic conductivity and bromine complexing ability.

The performance of HDES electrolytes was also compared with aqueous electrolytes, using a 1 M TBAB aqueous solution as a reference. To evaluate the cycle stability, a floating test was conducted by applying a constant voltage of 2 V for 240 h. This test provides valuable insights into the stability of the electrolyte and its ability to withstand the upper voltage limit of the applied nominal voltage.[31] The results of the floating test showed a capacity retention of 62% for the HDES-50 electrolyte and only 26.4% for the aqueous electrolyte (**Figure 4a**). The higher capacity retention observed for the HDES-50 electrolyte at 2 V highlights its superior electrochemical stability compared to the aqueous electrolyte. A floating test was also conducted for the 1 M KBr + 0.1 M TBAB aqueous electrolyte, where TBAB served as an additive (Figure S20, Supporting Information). In this case, capacity

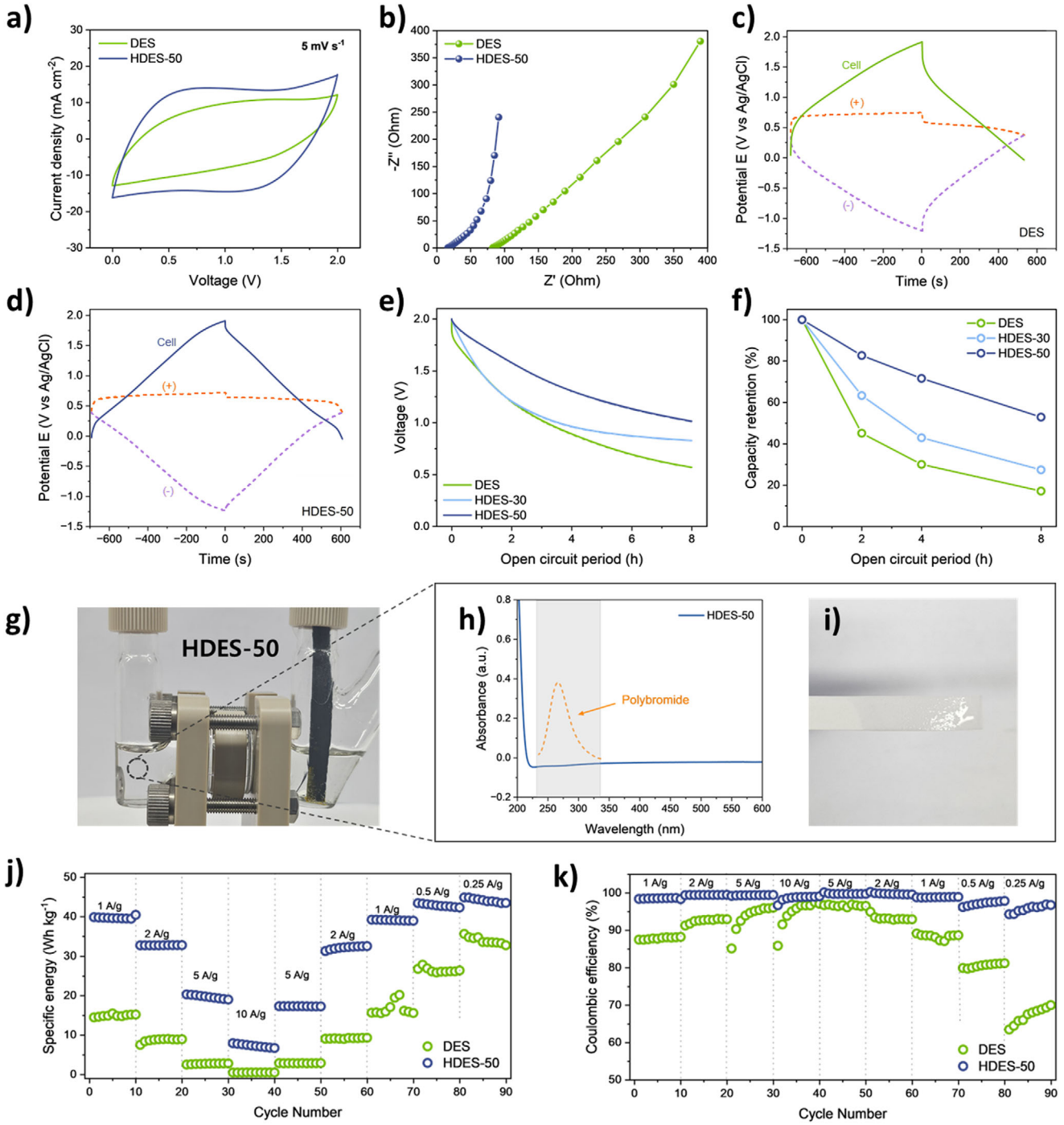

Figure 3. Performance comparison between DES and HDES. Two-electrode asymmetric cells (panels a, e, f, j, k) were constructed with DES and HDES electrolytes (3:1 negative-to-positive electrode mass ratio using AC carbon electrode). a) CV curves for each cell. b) Nyquist plots for each cell. GCD potential profiles of three-electrode asymmetric cells, divided into contributions from the positive electrode (orange curves) and the negative electrode (purple curves), are referenced to the centrally placed Ag/AgCl reference electrode (Figure S19, Supporting Information). Panels (c) and (d) correspond to the DES electrolyte and HDES-50 electrolyte, respectively. e) Voltage retention over 8 h under open-circuit conditions after charging. f) Open-circuit capacity retention for each cell, measured after charging and allowing the cell to rest at the open circuit for 2, 4, or 8 h, followed by complete discharge. g) Image of the H-type cell in the pre-charge state. h) KI paper test and i) UV–vis absorbance spectra of the HDES-50 electrolyte in the anode chamber, measured seven days after full charge. j) Discharge specific energy and k) Coulombic efficiency of each cell at various current densities ranging from 0.25 to 10 A g^{-1}.

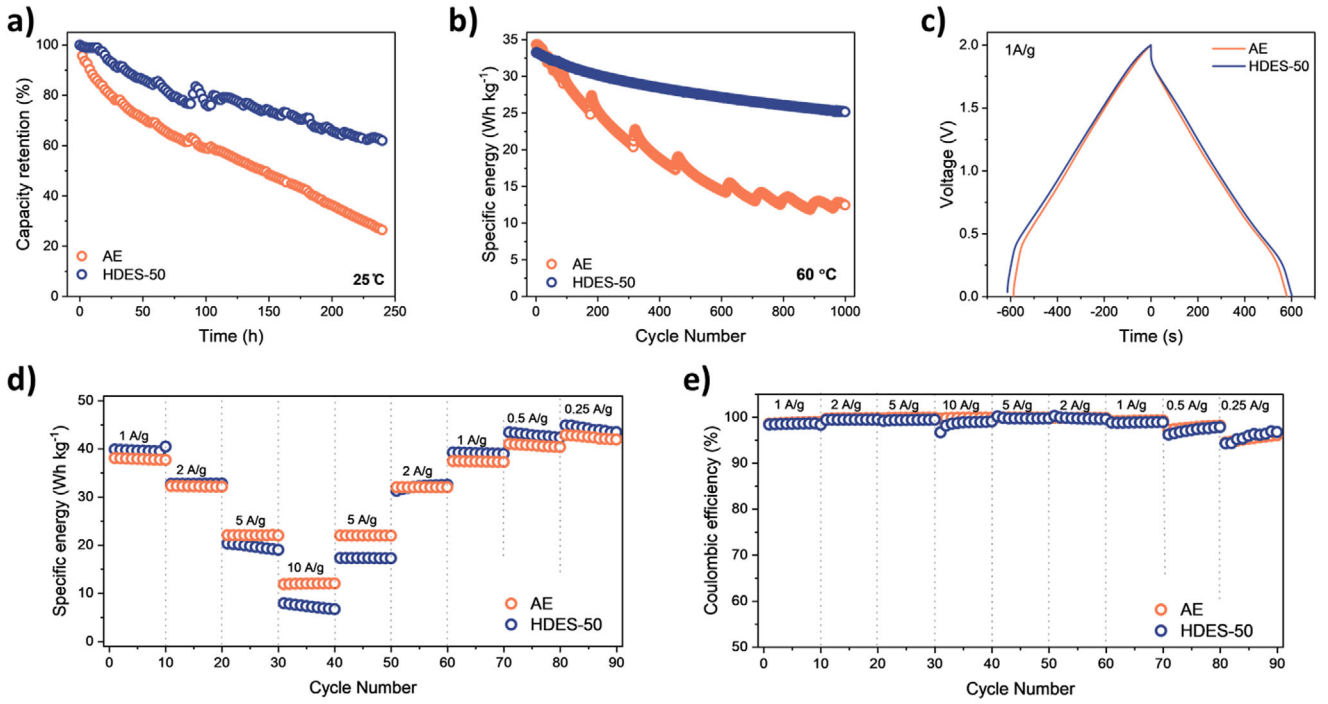

Figure 4. Performance comparison between the aqueous electrolyte and HDES. Two-electrode asymmetric cells were constructed with HDES and aqueous electrolytes (AE) (3:1 negative-to-positive electrode mass ratio using AC carbon electrode). a) Floating voltage test at 2 V. b) Cycle stability test at 2 V and 60 °C. c) GCD voltage profiles of each cell at 1 A g^{-1}. d) Discharge specific energy and e) Coulombic efficiency of each cell at various current densities ranging from 0.25 to 10 A g^{-1}.

retention dropped drastically to 20% within 100 h. These results emphasize that the hydrophobic nature of the TBA^+ in our HDES environment plays a critical role in inhibiting the HER and enhancing stability during extended voltage exposure.

To assess the thermal stability, a cycle test was conducted at 60 °C with a cutoff voltage of 2 V (Figure 4b). Elevated temperatures often accelerate electrolyte degradation under high operating voltages, and high volatility can lead to evaporation, contributing to a gradual decrease in energy storage capacity over cycles. The aqueous electrolyte exhibited an energy retention of only 36.1% after 1000 cycles with considerable fluctuations during cycling. In contrast, the HDES-50 electrolyte retained 75.7% of its initial charging capacity. This improved performance is attributed to the enhanced thermal stability of HDES-50, as shown in Figure 2e, compared to the aqueous electrolyte. To further evaluate the electrolytes, a rate capability test was conducted to assess coulombic efficiency and energy density. As shown in Figure 4c, GCD curves for both aqueous and HDES electrolytes displayed similar voltage profiles with no pronounced increase in IR drop at 1 A g^{-1}. The specific energy and coulombic efficiency of the HDES-50 electrolyte matched those of the aqueous electrolyte at lower current densities, except for high current densities exceeding 5 A g^{-1} (Figure 4d,e). These results demonstrate that the HDES matches the rate performance of aqueous electrolytes while offering superior thermal and electrochemical stability, effectively overcoming the limitations of aqueous electrolytes in energy storage applications.

In asymmetric cell configurations, where the capacitive electrode is oversized to match the capacity of the redox-enhanced electrode, the increased device mass reduces the mass-normalized specific energy. To fully realize the potential of redox-enhanced systems, redox ECs must concurrently utilize two separate redox couples, a catholyte, and an anolyte, each active at a different electrode and matching the redox activity of the other. This approach, known as a dual-redox EC, ensures enhanced energy utilization and efficiency.[3a]

To implement this strategy, we introduced BV as the anolyte due to its high solubility (>1.5 M) and reversible redox behavior to pair with the bromide catholyte.[3a,24b,32] The CV measurements in a beaker cell confirmed the occurrence of two-electron transfer reduction of BV from BV^{2+} to BV^0, with the first reduction ($BV^{2+} + e^- \rightarrow BV^{+\bullet}$) occurring at −0.62 V versus Ag/AgCl and the second reduction ($BV^{+\bullet} + e^- \rightarrow BV^0$) at −0.94 V versus Ag/AgCl (Figure S21, Supporting Information). The electrochemical behavior and stability of the HDES-50 electrolyte with the Br/BV dual redox couple were evaluated using two-electrode CV measurements at two cutoff voltages of 1.4 and 1.8 V (**Figure 5**a). The first profile (orange curve) corresponds to the voltage range where only the one-electron transfer reduction of BV occurs, while the second profile (blue curve) indicates the voltage range enabling the two-electron transfer reaction of BV. The CV measurements exhibited distinct peaks, confirming the effective redox activity of BV along with bromide oxidation within the HDES-50 electrolyte system in a dual-redox EC configuration.

To further investigate the individual redox reactions, a three-electrode cell was assembled, and a GCD test was carried out. At a cutoff voltage of 1.4 V, the redox reactions involving bromide at the cathode and viologen at the anode were clearly observed

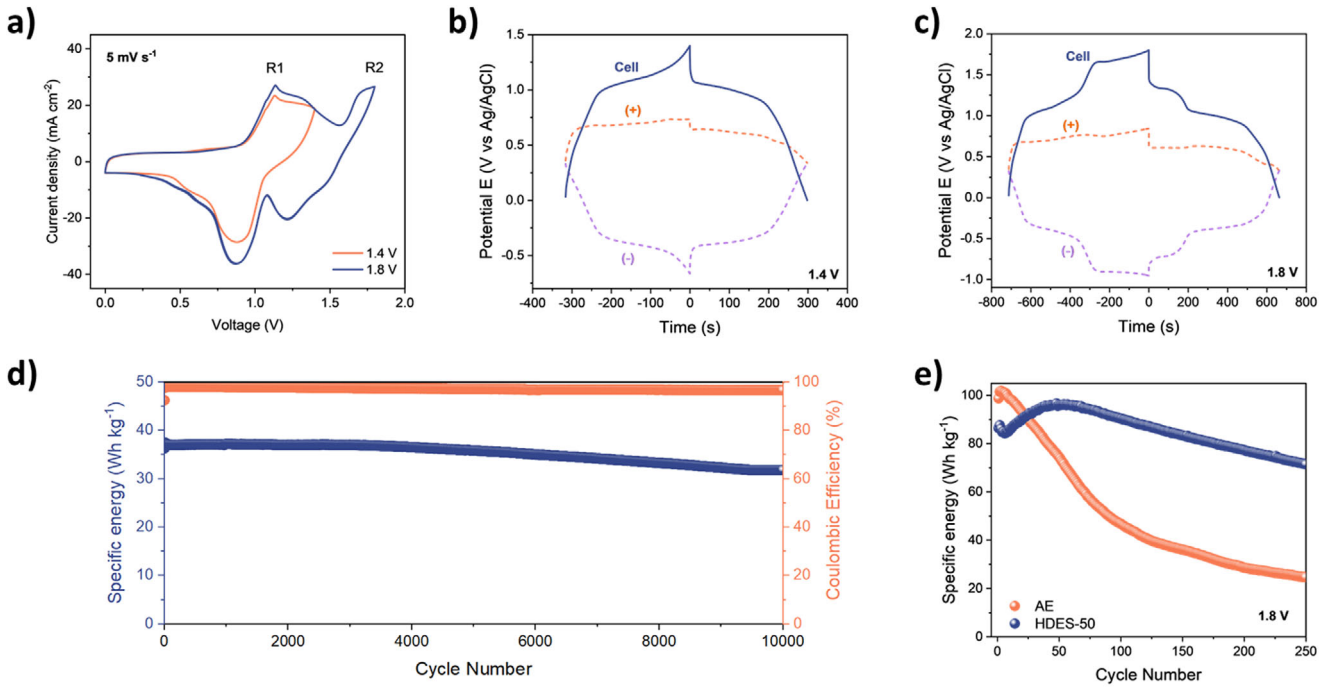

Figure 5. Performance of symmetric cells with HDES-50 electrolytes. Two-electrode symmetric cells (panels d and e) and three-electrode symmetric cells (panels a–c) were constructed with HDES-50 electrolytes. a) CV curves at different cutoff voltages. GCD potential profiles with the cutoff voltage of b) 1.4 V and c) 1.8 V. d,e) Cycling performance of dual redox ECs at a cutoff voltage of d) 1.4 V and e) 1.8 V. The initial rise in specific energy observed in Figure 5e (blue) can be attributed to the progressive wetting and stabilization (often referred to as the conditioning process) of the electrode–electrolyte interface during early cycling. For details, see Note S2 (Supporting Information).

(Figure 5b). When the cutoff voltage was increased to 1.8 V, the bromide redox reaction persisted at the cathode, while the viologen exhibited a two-electron transfer reaction at the anode, further confirming the dual-redox EC configuration (Figure 5c).

To evaluate the cycle performance, two-electrode symmetric cells were constructed using HDES-50 electrolytes with 1 M $BVBr_2$. The rate capability test showed that the HDES-50 electrolyte maintained coulombic efficiencies ranging from 96.4% to 99.8% across all tested current densities, from 0.5 to 10 A g^{-1}, indicating efficient charge and discharge processes (Figure S22, Supporting Information). Furthermore, in the long-term cycling test, the HDES-50 electrolyte exhibited an energy density of 36.3 Wh kg^{-1} and energy retention of over 87% after 10 000 cycles (1730 h) at a current density of 1 A g^{-1}. (Figure 5d).

Utilizing a two-electron transfer process is an effective strategy to increase energy density. However, the application of two-electron transfer in viologen derivatives (V^{2+}/V^0) in aqueous electrolytes faces challenges due to the limited operating voltage window and intrinsic stability issues of viologen, which are attributed to several well-established degradation mechanisms, such as irreversible dimerization of viologen radicals and precipitation of long-alkyl chain viologen derivatives in their zero-charge state (V^0) species.[33] In aqueous electrolytes, while the divalent (V^{2+}) and monovalent ($V^{+\bullet}$) forms of viologen are soluble, the zero-valent (V^0) form tends to precipitate.[3c] This insoluble, non-conductive zero-valent viologen can accumulate on the surface of the activated carbon electrodes, forming solid deposits that impede subsequent electrochemical reactions and reduce overall cell performance and stability. In contrast, the HDES-50 electrolyte facilitates the partial dissolution of V^0, preventing the formation of non-conductive deposits. To indirectly assess the solubility of zero-valent viologen in each electrolyte, we used a similarly structured bi-pyridine as a model and tested it in both the aqueous and HDES-50 electrolytes (Figure S23, Supporting Information). The results showed that bipyridine did not dissolve in the aqueous electrolyte, but it dissolved readily in the HDES-50 electrolyte, demonstrating the enhanced solubilizing capability of the HDES-50 system (Figure S24, Supporting Information). As shown in Figure 5e, the aqueous electrolyte retained only 24.2% of its energy after 250 cycles when charged at 1.8 V using the cell setup as in Figure 5d. In contrast, the HDES-50 electrolyte exhibited remarkably improved stability, achieving an energy density of 86.4 Wh kg^{-1} and retaining 82.7% of its energy over 250 cycles.

3. Conclusion

In this work, we designed a TBAB-based HDES that synergistically combines the advantages of aqueous and organic electrolytes for bromine-based energy storage systems. Unlike conventional HDES electrolytes, which incorporate only a small fraction of water and are ineffective at retaining the benefits of aqueous systems, our water-rich, DES-in-water system featuring hydrophobic TBAB achieves a compositionally distinct and optimized hydration level. A systematic evaluation of hydration levels confirmed that HDES-50 provides an optimal balance of electrochemical stability, ionic conductivity, and effective suppression of charged bromine cross-diffusion through solid complexation, minimizing self-discharge. These properties establish HDES-50

as a versatile electrolyte that bridges aqueous and non-aqueous systems, harnessing their respective advantages while mitigating inherent limitations.

The optimized HDES-50 demonstrated superior performance metrics across multiple tests. It exhibited higher energy density and coulombic efficiency compared to traditional DES, retaining 75.7% of its initial capacity after 1000 cycles at 60 °C, whereas the aqueous electrolyte retained only 36.1%. In dual-redox configurations with BV anolyte, the HDES-50 electrolyte achieved an energy density of 36.3 Wh kg^{-1} with 87% capacity retention over 10 000 cycles. Additionally, it reached 86.4 Wh kg^{-1} at 1.8 V by utilizing the two-electron transfer of viologen. These findings establish HDES-50 as a promising electrolyte for bromine-based redox ECs, offering a compelling combination of stability, efficiency, and long-term performance. Furthermore, by leveraging these insights, the water-rich HDES design paves the way for next-generation energy storage technologies.

Supporting Information

Supporting Information is available from the Wiley Online Library or from the author.

Acknowledgements

T.P.E. and G.L. contributed equally to this work. This research was supported by the National Research Foundation of Korea (NRF) grant funded by the Korean government (MSIT) (RS-2024-00347887).

Conflict of Interest

The authors declare no conflict of interest.

Data Availability Statement

The data that support the findings of this study are available in the supplementary material of this article.

Keywords

DES-in-water electrolytes, hydrated deep eutectic solvents, redox electrolytes, redox-enhanced electrochemical capacitors

Received: December 9, 2024
Revised: February 15, 2025
Published online: March 27, 2025

[1] a) J. Yan, Q. Wang, T. Wei, Z. Fan, *Adv. Energy Mater.* **2014**, *4*, 1300816; b) J. Zhao, A. F. Burke, *J. Energy Chem.* **2021**, *59*, 276.
[2] J. Zhang, M. Gu, X. Chen, *Micro and Nano Eng.* **2023**, *21*, 100229.
[3] a) B. Evanko, S. W. Boettcher, S. J. Yoo, G. D. Stucky, *ACS Energy Lett.* **2017**, *2*, 2581; b) J. Byeon, J. Ko, S. Lee, D. H. Kim, S. W. Kim, D. Kim, W. Oh, S. Hong, S. J. Yoo, *ACS Energy Lett.* **2023**, *8*, 2345; c) H. Luo, G. Wang, J. Lu, L. Zhuang, L. Xiao, *ACS Appl. Mater. Interfaces* **2019**, *11*, 41215.
[4] a) Q. Li, M. Haque, V. Kuzmenko, N. Ramani, P. Lundgren, A. D. Smith, P. Enoksson, *J. Power Sources* **2017**, *348*, 219; b) S. J. Yoo, B. Evanko, X. Wang, M. Romelczyk, A. Taylor, X. Ji, S. W. Boettcher, G. D. Stucky, *J. Am. Chem. Soc.* **2017**, *139*, 9985; c) B. Hwang, J. Yang, D. Kim, W. C. Yun, J. W. Lee, *Electrochim. Acta* **2023**, *442*, 141871.
[5] J. H. Lee, Y. Byun, G. H. Jeong, C. Choi, J. Kwen, R. Kim, I. H. Kim, S. O. Kim, H. T. Kim, *Adv. Mater.* **2019**, *31*, 1904524.
[6] a) A. Mahmood, Z. Zheng, Y. Chen, *Adv. Sci.* **2023**, 2305561; b) H. Park, G. Park, S. Kumar, H. Yoon, J. Baek, T. Tamulevičius, S. Tamulevičius, H.-J. Kim, *J. Power Sources* **2023**, *580*, 233212; c) E. Lancry, B.-Z. Magnes, I. Ben-David, M. Freiberg, *ECS Trans.* **2013**, *53*, 107.
[7] a) L. Gao, Z. Li, Y. Zou, S. Yin, P. Peng, Y. Shao, X. Liang, *Iscience* **2020**, 23; b) Y. Choi, J. Hwang, K. Kim, S. Jana, S. U. Lee, J. Chae, J. Chang, *Anal. Chem.* **2019**, *91*, 5850; c) B. Evanko, S. J. Yoo, J. Lipton, S.-E. Chun, M. Moskovits, X. Ji, S. W. Boettcher, G. D. Stucky, *Energy Environ. Sci.* **2018**, *11*, 2865; d) Y. Lim, G. Lee, J. H. Kim, J. K. Seo, S. J. Yoo, *Energy Storage Mater.* **2024**, *68*, 103331.
[8] a) Q. Nian, X. Zhang, Y. Feng, S. Liu, T. Sun, S. Zheng, X. Ren, Z. Tao, D. Zhang, J. Chen, *ACS Energy Lett.* **2021**, *6*, 2174; b) K. Xu, C. Wang, *Nat. Energy* **2016**, *1*, 16161.
[9] a) M. Chen, Y. Zhang, G. Xing, S.-L. Chou, Y. Tang, *Energy Environ. Sci.* **2021**, *14*, 3323; b) H. Wang, Z. Chen, Z. Ji, P. Wang, J. Wang, W. Ling, Y. Huang, *Mater. Today Energy* **2021**, *19*, 100577.
[10] a) E. L. Smith, A. P. Abbott, K. S. Ryder, *Chem. Rev.* **2014**, *114*, 11060; b) S. Azmi, M. F. Koudahi, E. Frackowiak, *Energy Environ. Sci.* **2022**, *15*, 1156; c) M. Zhong, Q. F. Tang, Y. W. Zhu, X. Y. Chen, Z. J. Zhang, *J. Power Sources* **2020**, *452*, 227847.
[11] a) R. Chen, C. Zhang, J. Li, Z. Du, F. Guo, W. Zhang, Y. Dai, W. Zong, X. Gao, J. Zhu, *Energy Environ. Sci.* **2023**, *16*, 2540; b) Y. Zhong, X. Xie, Z. Zeng, B. Lu, G. Chen, J. Zhou, *Angew. Chem., Int. Ed.* **2023**, *62*, 202310577; c) W. Yang, X. Du, J. Zhao, Z. Chen, J. Li, J. Xie, Y. Zhang, Z. Cui, Q. Kong, Z. Zhao, *Joule* **2020**, *4*, 1557.
[12] Y.-R. Tsai, B. Vedhanarayanan, T.-Y. Chen, Y.-C. Lin, J.-Y. Lin, X. Ji, T.-W. Lin, *J. Power Sources* **2022**, *521*, 230954.
[13] a) M. C. Gutiérrez, M. L. Ferrer, C. R. Mateo, F. del Monte, *Langmuir* **2009**, *25*, 5509; b) E. Posada, M. Roldán-Ruiz, R. J. Riobóo, M. Gutiérrez, M. Ferrer, F. Del Monte, *J. Mol. Liq.* **2019**, *276*, 196; c) H. Zhang, M. L. Ferrer, R. J. Jimenez-Rioboo, F. del Monte, M. C. Gutierrez, *J. Mol. Liq.* **2021**, *329*, 115573.
[14] A. Basaiahgari, S. Panda, R. L. Gardas, *J. Chem. Eng. Data* **2018**, *63*, 2613.
[15] S. Zhu, H. Li, W. Zhu, W. Jiang, C. Wang, P. Wu, Q. Zhang, H. Li, *J. Mol. Graph. Model.* **2016**, *68*, 158.
[16] a) H. Wang, S. Liu, Y. Zhao, J. Wang, Z. Yu, *ACS Sustainable Chem. Eng.* **2019**, *7*, 7760; b) D. Wu, L. H. Xu, H. J. Feng, Y. W. Zhu, X. Y. Chen, P. Cui, *J. Power Sources* **2021**, *492*, 229634; c) X. Zhang, Y. Zhou, Y. Gong, Y. Huang, C. Sun, *Chem. Phys. Lett.* **2017**, *678*, 233.
[17] Q. Zhang, K. D. O. Vigier, S. Royer, F. Jérôme, *Chem. Soc. Rev.* **2012**, *41*, 7108.
[18] Y. Xie, J. Huang, T. Kong, X. Zhou, K. Wu, X. Liu, J. Yi, L. Xing, Y. Xia, *Energy Storage Mater.* **2023**, *56*, 218.
[19] A. S. Ferreira, R. Craveiro, A. R. Duarte, S. Barreiros, E. J. Cabrita, A. Paiva, *J. Mol. Liq.* **2021**, *342*, 117463.
[20] a) H. Zhang, M. L. Ferrer, M. J. Roldán-Ruiz, R. J. Jiménez-Riobóo, M. a. C. Gutiérrez, F. Del Monte, *J. Phys. Chem. B* **2020**, *124*, 4002; b) E. Posada, N. López-Salas, R. J. Riobóo, M. L. Ferrer, M. C. Gutiérrez, F. Del Monte, *Phys. Chem. Chem. Phys.* **2017**, *19*, 17103; c) M. Roldán-Ruiz, R. Jiménez-Riobóo, M. Gutiérrez, M. Ferrer, F. del Monte, *J. Mol. Liq.* **2019**, *284*, 175.
[21] A. Gertrudes, R. Craveiro, Z. Eltayari, R. L. Reis, A. Paiva, A. R. C. Duarte, *ACS Sustainable Chem. Eng.* **2017**, *5*, 9542.
[22] A. Zhou, J. Zhang, M. Chen, J. Yue, T. Lv, B. Liu, X. Zhu, K. Qin, G. Feng, L. Suo, *Adv. Mater.* **2022**, *34*, 2207040.

[23] a) K. Guan, L. Tao, R. Yang, H. Zhang, N. Wang, H. Wan, J. Cui, J. Zhang, H. Wang, H. Wang, *Adv. Energy Mater.* **2022**, *12*, 2103557; b) N. Dubouis, A. Serva, R. Berthin, G. Jeanmairet, B. Porcheron, E. Salager, M. Salanne, A. Grimaud, *Nat. Catal.* **2020**, *3*, 656; c) N. Dubouis, A. Serva, E. Salager, M. Deschamps, M. Salanne, A. Grimaud, *J. Phys. Chem. Lett.* **2018**, *9*, 6683.

[24] a) K. Hoshino, M. Ando, Y. Oikawa, M. Okuma, K. Murashiro, *Sol. Energy Mater. Sol. Cells* **2015**, *137*, 15; b) B. Evanko, S. J. Yoo, S.-E. Chun, X. Wang, X. Ji, S. W. Boettcher, G. D. Stucky, *J. Am. Chem. Soc.* **2016**, *138*, 9373.

[25] X. Chen, M. A. Rickard, J. W. Hull Jr, C. Zheng, A. Leugers, P. Simoncic, *Inorg. Chem.* **2010**, *49*, 8684.

[26] a) R. S. Nicholson, *Anal. Chem.* **1965**, *37*, 1351; b) N. Elgrishi, K. J. Rountree, B. D. McCarthy, E. S. Rountree, T. T. Eisenhart, J. L. Dempsey, *J. Chem. Educ.* **2018**, *95*, 197.

[27] D. Han, C. Cui, K. Zhang, Z. Wang, J. Gao, Y. Guo, Z. Zhang, S. Wu, L. Yin, Z. Weng, *Nat. Sustain.* **2022**, *5*, 205.

[28] J. Yu, C. Yu, X. Song, Q. Zhang, Z. Wang, Y. Xie, Y. Liu, W. Li, Y. Ding, J. Qiu, *J. Am. Chem. Soc.* **2023**, *145*, 13828.

[29] H. Yang, S. Lin, Y. Qu, G. Wang, S. Xiang, F. Liu, C. Wang, H. Tang, D. Wang, Z. Wang, *Adv. Sci.* **2024**, *11*, 2307780.

[30] M. F. Bento, L. Thouin, C. Amatore, *J. Electroanal. Chem.* **1998**, *446*, 91.

[31] L. Köps, F. A. Kreth, D. Leistenschneider, K. Schutjajew, R. Gläßner, M. Oschatz, A. Balducci, *Adv. Energy Mater.* **2023**, *13*, 2203821.

[32] S. Sathyamoorthi, M. Kanagaraj, M. Kathiresan, V. Suryanarayanan, D. Velayutham, *J. Mater. Chem. A* **2016**, *4*, 4562.

[33] C. DeBruler, B. Hu, J. Moss, X. Liu, J. Luo, Y. Sun, T. L. Liu, *Chem* **2017**, *3*, 961.